mechanical bridge machineries: phenomenological modelling and experiments

Journal of Physics: Conference Series **2647** (2024) 042008 doi:10.1088/1742-6596/2647/4/042008

Mechanical bridge machineries: Phenomenological modelling and experiments

K Sektani[1], A Tsouvalas[1], and A Metrikine[1]

[1]Department of Engineering Structures, Delft University of Technology, Stevinweg 1, 2628 CN Delft, The Netherlands

k.sektani@tudelft.nl

Abstract. The reassessment of existing mechanical bridge machineries in The Netherlands has prompted the development of acceptance/rejection criteria for evaluating their structural safety. The current design code in The Netherlands [1, 2] establishes an ultimate limit state, primarily intended for the design of new machineries, employing a conservative approach with upper bounds on maximum loads. However, to reassess existing bridges and prevent unnecessary replacements, a more accurate prediction of the dynamic response is essential. The current code relies on a linear single degree of freedom (SDOF) dynamical system [3], which is found to inadequately predict the dynamic response of existing machineries across all load cases [4]. This discrepancy can be attributed to, for instance, the neglect of time-dependent and discontinuous model parameters of the machineries [5, 6, 7]. Given that each movable bridge possesses a unique set of fixed parameters, on-site measurements of a single bridge do not provide the generic information required for the design and/or reassessment of existing structures in general terms. In this paper, a novel experimental setup is presented which allows the investigation of a wide range of variations in order to capture the dynamics of the powertrain in a class of bridge machineries. Additionally, a modelling methodology is developed to overcome the limitations of existing calculation rules, by incorporating base excitations, damping, and other relevant variables of the physical system, which are currently neglected by the code. A subsequent comparison with measured data, demonstrating the accuracy of the proposed methodology for different driveline compositions, machinery configurations and braking systems is included in the thesis of this research, due to page limitations.

1. Introduction

The calculation rules in the current Dutch standard, NEN 6786-1:20017+C1:2021 Rules for the Design of Movable Bridges, are based on a linear semi-definite system , subjected to quasi-static loads such as the maximum motor and braking torques. Therefore, the behavior of this dynamical system is characterized by the motion caused by given excitations in the form of externally applied forces. Subsequently, the code defines an ultimate limit state during various load cases based on this model.

Observations show that the model falls short in accurately describing the behavior of the movables as a dynamical system subjected to given excitations in the form of initial velocities [8, 9, 10]. There is a suspicion that the current calculation rules are overly conservative, resulting in underutilization of the remaining lifespan of existing bridge machineries when they are reassessed.

In order to investigate the dynamic behavior of movables a novel experimental setup is presented in this paper; one that allows a large number of variations with the purpose of capturing the dynamics of bridge operating machineries during various load situations, such as normal operation and emergency braking.

The purpose of the laboratory experiments is to investigate the effect of these relevant variables on the system response and to verify a developed numerical model methodology. Based on this verified methodology, suitable dynamical models can be identified for various driveline compositions, machinery configurations, braking systems and load situations by means of comparison with measured data. The dynamical models account for base excitations, damping, and other time-varying variables.

This paper is structured as follows: In the Methods section, we present the design of a novel experimental setup for investigating movable bridge dynamics. We provide details on the experimental design, variables considered, and the experimental matrix. Moving to the Results section, we compare the proposed model methodology with measured data, focusing on accurately determining dynamic forces in the powertrain. Additionally, we analyze and compare torque measurements from the motor shaft and other driveline locations. In the Discussion section, we interpret the experimental outcomes, discussing differences between 2-DOF and multi-DOF systems in capturing powertrain dynamics and highlighting the relevance of torque measurements for assessing machineries. Finally, in the Conclusions section, we summarize key findings and emphasize the importance of developing calculation models for movables with diverse component compositions and load situations. Our proposed methodology validates theoretical models using in situ measurements, employing a similar phenomenological approach.

2. Methods

A unique test rig is built in the Construction Laboratory II (Stevin lab II) of the Faculty of Civil Engineering and Geosciences (CEG) at Delft University of Technology in the Netherlands. With this test rig dynamic loads in movable bridge machineries are experimentally simulated and measured during different load situations, such as normal operation and emergency brake. The setup allows the investigation of different sets of parameters in order to provide generic measurement data that one needs for developing and verifying theoretical models to capture the dynamics of movables. The test rig is representing drawbridges and bascule bridges that are counterbalanced and open by pivoting around a horizontal axis and which are mechanically driven. The operating system uses mechanical power transmission components, such as, gears and gear carrying shafts to couple the prime mover to the movable span.

Contrary to the past, when all prime movers were torque controlled (for instance by squirrel cage and slip ring motors), nowadays, electro-technical developments made it possible to adjust the position and speed of the bridge smoothly using electrical controls. Therefore, a prime mover is chosen for the test rig, that like almost all bridge machineries, is speed regulated by means of a frequency converter. The converter is used for speed control of AC motors and allows the motor speed to be controlled. Also, in case of braking, two common mechanical brake types are used, namely, a built-in disk brake with friction clutches and a thruster brake.

In the following section the design of the setup, consisting of mechanical components, the variables and used sensors as well as the experimental matrix are presented.

3. Design of the experiment

The test rig consists of various drive components as shown in Figure 1, such as the motor drive (1), flywheels (2 and 15), gearboxes (3,6 and 14), couplings (4) and interchangeable shafts S1 and S2 (respectively, 5 and 13).

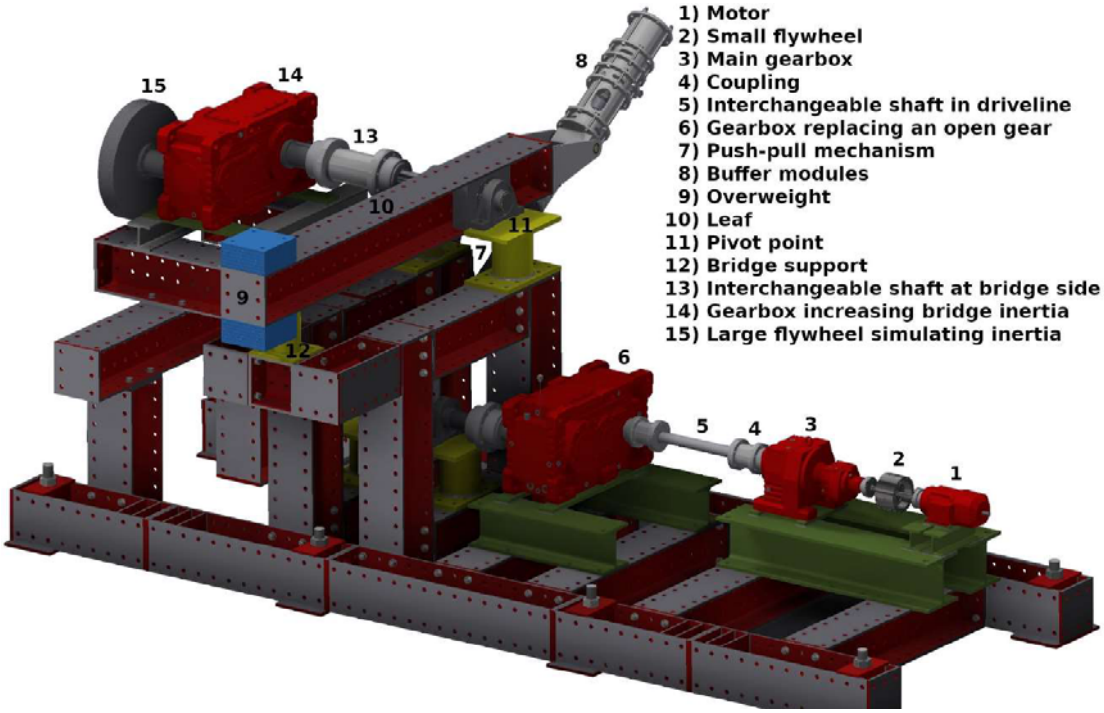

Figure 1. 3D Inventor model of the test rig

All these components are commonly used in on-site movable bridge machineries. However, for the sake of simplicity and cost effectiveness, some parts are replaced by comparable components with similar functions. For instance, because of lack of room in the laboratory, the bridge leaf is represented by means of a lever beam (10) cantilevered at one end on a pivot point (11) and driven by a crank-connecting rod mechanism (7).

Also, at the tip of the beam there is a dead weight (9) placed, which represents the overweight or imbalance, calculated as the weight of a span (or leaf) of a movable bridge minus the counterweight. Moreover, a sizable flywheel (15) will compensate for the inertia of the leaf and the ballast, as they are not incorporated in the design, because of space limitations of the laboratory. The final gearbox (14) will result in an equivalent inertia for the leaf and ballast, which is as high as the inertia of the large flywheel times the ratio of the final gearbox squared. The final gearbox is connected with an interchangeable hollow shaft (13) to the leaf, which represents an equivalent stiffness of the movable bridge span. The crank-connecting rod mechanism (7), as shown in Figure 2, is the final connection of the drivetrain to the simple trunnion bascule bridge structure, which is a swing arm mechanism combined with a closed gearbox (6). The crank is directly connected to the output shaft of the gearbox and hingedly attached to the connecting push-pull rod, which in turn, is hinged to the leaf girder (10). The position of the push-pull rod is oriented so it is aligned with the crank when the bridge is closed, which pushes and pulls the back side of the beam.

Also a buffer-unit (8) is specifically designed for this test rig, which consists of three different modules. The first one is to contain spring discs, similar to spring buffers used in bridge machineries and the other two modules are to simulate friction and clearance as independent variables in the drivetrain.

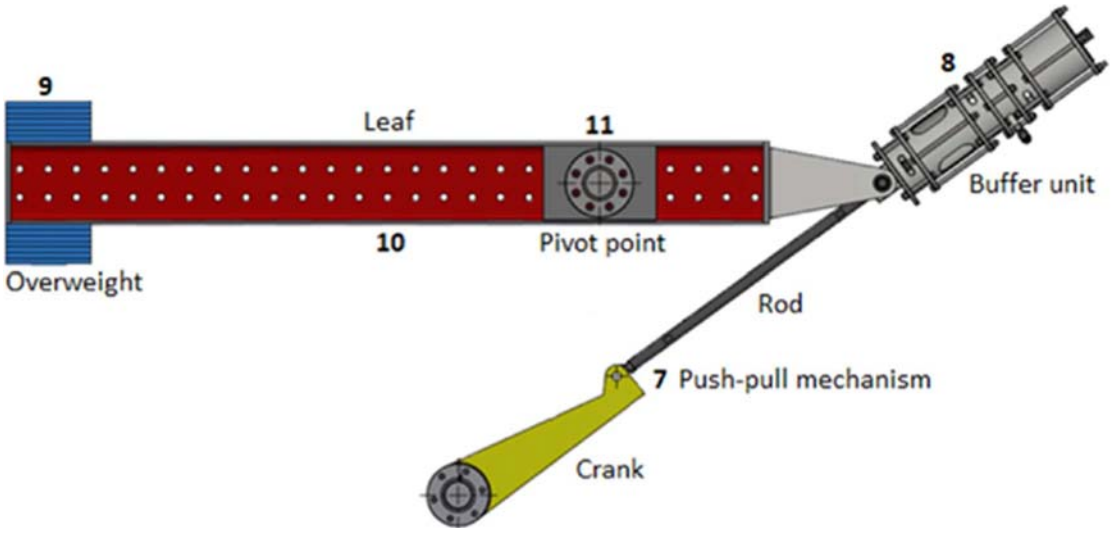

Figure 2. The push-pull mechanism in accordance with the design as shown in Figure 1.

As with any experimental study, there are independent, dependent, and controlled variables. The *independent variables* are the input variables that are manipulated. In this experimental study the independent variables are shown in Table 1.

Table 1. Manipulated independent variables with associated part numbers (PN), symbol and unit.

No.	Variable	Part	PN	Symbol	Unit
1	Rotational speed	Motor	1	v_{Jm}	rpm
2	Inertia J1	Small flywheel	2	$m_{1,2}$	kg.m^2
3	Torsional stiffness S1	Solid shaft in drivetrain	5	$k_{2,2}$	Nm/rad
4	Torsional stiffness S2	Hollow shaft at bridge side	13	k_3	Nm/rad
5	Overweight	On tip lever beam	9	$m_{2,2}$	kg.m^2
6	Inertia J3	Large flywheel	15	m_3	kg.m^2
7	Angle of opening	Leaf	10	x_{J2}	deg
8	Clearance	Buffer module 1	8	u_{in}	mm
9	Friction	Buffer module 2	8	f_w	kN
10	Translational stiffness	Buffer module 3	8	k_b	N/m
11	Braking time	Disc brake	1	t_{br}	s
12	Braking torque	Thruster brake	2	M_{br}	V (Nm)

The controlled constant variables do not change. These may influence the outcome of the experiment, but since they are held constant, their contribution is not considered. These are transmission factors, backlashes and efficiencies in gearboxes (3, 6 and 14), friction in bearings and other rotating parts, overall damping, and the torsional stiffness of other parts, beside the variable shafts (5 and 13), such as the torsional stiffness of the motor shaft between (1) and (2).

The dependent variables are measured and with each measurement values will change as the independent variables are altered. The measured quantities and parameters are listed below in Table 2. Also the used sensor, location, symbol and unit of these dependent variables are included in the table. The dependent variables are mainly the torsional moments at different locations in the powertrain, however, also some other dependent variables are measured.

Table 2. Measured dependent variables with associated sensor, location, symbol and unit.

No.	Variable	Sensor	PN	Symbol	Unit
1	Torsional moment of motor shaft	Strain gauges	1 - 2	$M1_{J1}$	Nm
2	Torsional moment of motor shaft	Strain gauges	2 - 3	$M2_{J1}$	Nm
3	Torsional torque of variable shaft S1	Strain gauges	4	$M3_{S1}$	Nm
4	Torsional torque of crankshaft	Strain gauges	6 - 7	$M4_{J2}$	Nm
5	Torsional moment of variable shaft S2	Strain gauges	13	$M5_{S2}$	Nm
6	Angle of lever beam	String potentiometer	10	x_{J2}	deg
7	Angular displacement of crankshaft	String potentiometer	6 - 7	x_{CS}	deg
8	Angular displacement of connecting rod	Angle sensor	7	x_{SR}	deg
9	Angular speed of large flywheel	Hall Sensor	15	v_{J3}	deg
10	Force in connecting rod	Strain gauges	7	F_{SR}	kN

Table 3 Registered dependent variables with associated sensor, location, symbol and unit.

No.	Variable	Sensor	PN	Symbol	Unit
11	Motor speed	Output FC (given)	1	v_{Jm}	rpm
12	Current motor	Output FC (given)	1	I_{Jm}	A
13	Set value of friction module	Load cell	8	F_{Buf}	kN
14	Measured compression spring module	String potentiometer	8	u_{out}	mm
15	Set value clearance module	String potentiometer	8	u_{in}	mm

4. Experimental matrix

An experimental matrix consists of the input of independent variables for the measurements and is an important aspect of the experimental research. The input variables are quantified and selected in such a way that they show a measurable effect, taking into account the measuring range of the sensors. In addition, the step size for each variable has been carefully chosen so that it can be easily adjusted when measuring.

For instance, the inertia of the large flywheel is manipulated by varying the number of discs from which the flywheel is consisting. On the one hand, the range of the inertia should be comparable to inertia of real movable bridges. On the other hand, the discs are dimensioned in such a way that they can be easily exchanged in terms of size and weight. Therefore, the experimental matrix is shown in Table 4 is made after careful consideration and mathematical explorations during the design of the test rig, which takes into account the measuring range of the sensors, the effect to be measured on the dependent variables and the feasibility of the measurements. Moreover, a total of six operating conditions 'load situations' (ls) were measured, namely normal operation opening (O_VTD), normal operation closing (C_VTD), hard emergency stop opening (O_NS0), hard emergency stop closing 'Close' (C_NS0), soft emergency stop opening (O_NS1) and soft emergency stop closing (C_NS1). Various measurement sessions are carried out, each focusing on one independent variable.

Given the maximum page limit of this article, it is important to acknowledge the constraints regarding the presentation of these detailed information given in the tables. Due to these limitations, some specific details related to the input variables, research methodology and analysis are not fully expounded upon in this paper. However, it is essential to note that the provided information is comprehensive enough to facilitate a thorough understanding and assessment of the obtained results, mentioned in the following section.

Table 4. Experimental matrix.

Variable	Symbol							Unit
Load situations	ls	O_VTD	C_VTD	O_NS0	C_NS0	O_NS1	C_NS1	
Velocity motor	v_{jm}	200	400	600	800	1000		rpm
Inertia small flywheel	$m_{1,2}$	0,032	0,049	0,066	0,083	0,100	0,116	kg.m^2
Stiffness shaft 1 (S1)	$k_{2,2}$	4,00	12,6	30,8	63,8	118		Nm/rad
Stiffness shaft 2 (S2)	$k_{3,2}$	3,00	4,19	5,65	7,42	9,53		Nm/rad
Inertia large flywheel	m_3	0,06	2,81	5,57	8,32	11,1	13,8	kg.m^2
Clearances	u_{in}	0	1	2	3	4	8 and 12	mm
Friction force	f_w	0	0,4	0,9	1,3	1,7		kN
Friction force	f_w	0	2,1	4,2	6,3			kN
Angle of braking	x_{J2}	-	5	25	45	65	85	deg
Braking time	t_{br}	-	1,0	1,5	2,0	2,5	3,0	s
Braking torque	M_{br}	-	30	40	50	60		V (Nm)

Table 5. Parameters of the test rig as a dynamic 3-DOF system.

Variable	Symbol	PN	Value	Unit
Inertia 1st DOF; rotor, coupling and small flywheel	m_1	1 - 2	0,125	kg.m^2
Equivalent stiffness k_1 of motor shaft	k_1	1 - 2	19203	Nm/rad
Corresponding damping constant for given k_1	c_1		10,4	Nm.s/rad
Inertia 2nd DOF; overweight and leaf	m_2	9 & 10	0,0003	kg.m^2
Equivalent stiffness k_2 reduced to motor shaft	k_2	6, 7 & 8	0,84	Nm/rad
Corresponding damping constant for given k_2	c_2		0,003	Nm.s/rad
Inertia 3rd DOF; large flywheel	m_3	15	0,20	kg.m^2
Equivalent stiffness k_3 reduced to motor shaft	k_3		0,10	Nm/rad
Corresponding damping constant for given k_3	c_3		0,03	Nm.s/rad
Damping ratio of structural damping in the system	ζ		0.106	-
Transmission ratio gearbox 1 (GB1)	N_1	3	227	-
Transmission ratio gearbox 2 (GB2)	N_2	6	8,21	-
Transmission ratio gearbox 3 (GB3)	N_3	14	203,25	-

5. Results

This section compares the results of using a 2-DOF system versus a multi-DOF system and presents measurements of torsion moments at different locations in the powertrain.

5.1 Results of 2-DOF versus multi-DOF system

A sensitivity analysis of the number of degrees of freedom shows that using calculation models with more than two degrees of freedom does not add value to the accuracy of the results compared to a model with two degrees of freedom, in accordance to the theory as mentioned by Stroosma [3]. This means that with a dynamic system of two degrees of freedom, the movement of a movable bridge can be properly described. On the one hand, the motor shaft and attached parts are concentrated to one mass moment of inertia m_1 at the drive side as a rigid body. On the other hand, the movable span and counterweight together form a second mass moment of inertia m_2 at the driven side. Furthermore, the reduced inertias of the other components in the powertrain to the motor shaft, such as intermediate shafts, couplings and gears, are negligibly small compared to these two concentrated inertias m_1 and m_2. This

is because of the transmission ratios of the gears in the powertrain. However, these intermediate parts can be included in the modeling as massless springs in order to consider their stiffness as part of the physical system.

Figure 3 shows experimentally that even the contribution of the lever beam and the overweight is negligible as additional inertia, compared to the large flywheel. The gravity M_{F2} (yellow line) plus an externally applied torque, caused by the large flywheel $M5_{S2}$ (orange line), are almost equal to the measured dynamic torque in the interchangeable shaft $M3_{S1}$ (blue line). There is still a small difference to be noticed between this two torques, when the system starts to accelerate or decelerate because of the mass moment of inertia of the lever beam and attached overweight. However, the mass moment of inertia of the intermediate parts are relatively much smaller, than the lever beam with its attached overweight, as designed in the test rig.

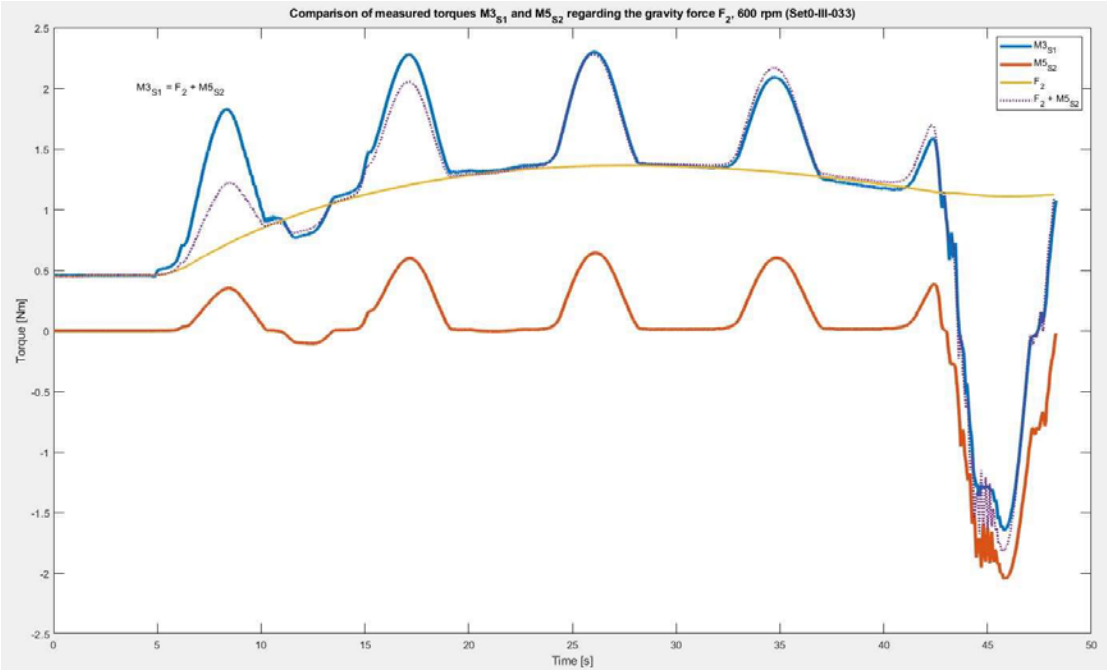

Figure 3. Measured $M5_{S2}(t)$ (orange line) added to the gravity force $M_{F2}(t)$ and modeled torque in the motor shaft $M1_{J1}(t)$.

5.2 Measured torque in motor shaft compared to other locations in powertrain

The applied torque to stop the rotor by a built-in brake system with friction clutches causes a short-term peak force $M1_{J1}$ in the motor shaft, just before the flywheel. This dynamic peak force, as shown in Figure 4 with an orange line, occurs as a result of change in the motion of the mass moment of inertia m_1 on the drive side, consisting mainly of inertia of the small flywheel. This peak torque does not have time to propagate to the rest of the drivetrain, as the motor shaft and attached parts come to a standstill very quickly (usually in less than a second). However, due to the flexibility of the powertrain, after application of the brake and stopping the rotor, the bridge deck is still moving. This creates a second peak in the motor shaft, which is held by the brake at that moment. This second peak is caused by the deceleration of the inertia at the bridge-side (and not by the braking torque) and it is considerably lower than the first peak. It is important to notice that the dynamic force, causing the second lower peak in the motor shaft, results in the first occurring peak in the rest of the drivetrain, as shown in the figure below. Contrary to the motor shaft, the measured torques in the following locations show one peak during the

braking: In the intermediate shaft $M2_{J1}$ (yellow line), in the solid interchangeable shaft S1 $M3_{S1}$ (purple line) and in the crank shaft $M4_{J2}$ (green line).

The dotted blue line in the plot is the closing moment caused by the gravity moment on the leaf M_{F2}. The blue line is the torque measured in the hollow interchangeable shaft S2 $M5_{S2}$, which is caused by change in motion of the large flywheel. Once again, it can be noticed that the sum of the gravity moment M_{F2} and the torque caused by inertia of the large flywheel $M5_{S2}$ almost equates the torques measured in other locations of the powertrain ($M2_{J1}$, $M3_{S1}$ and $M4_{J2}$). The small differences are caused due to friction in the gearboxes.

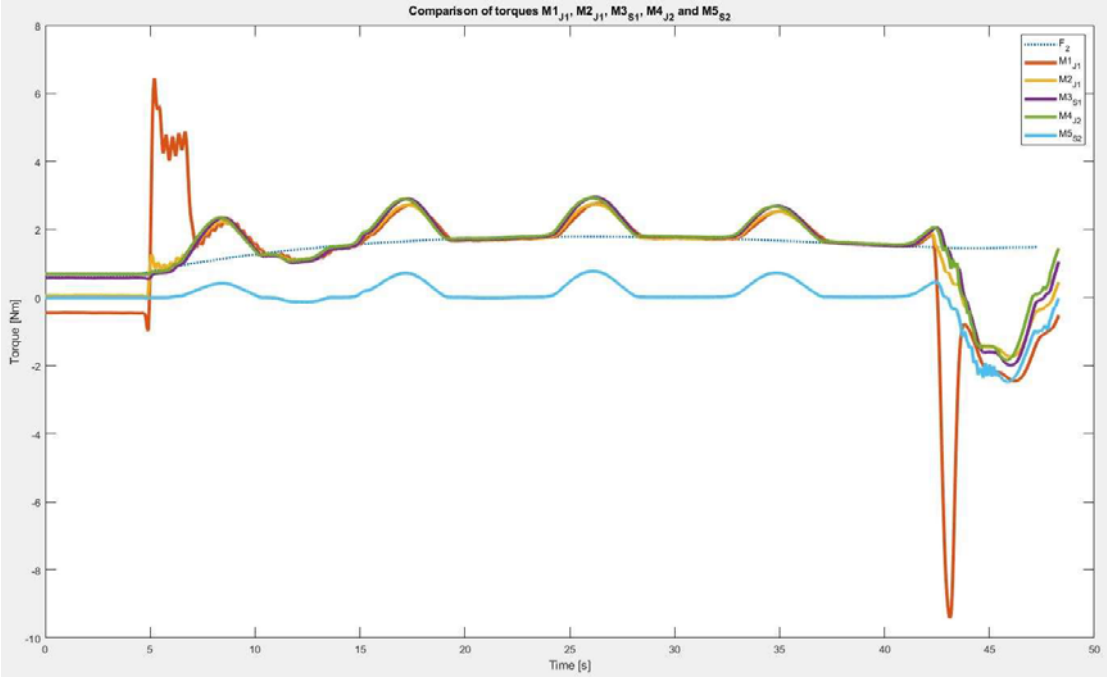

Figure 4. Comparison of measured torques in the powertrain at different locations: Measured torque in the motor shaft $M1_{J1}(t)$ (orange line), intermediate shaft $M2_{J1}(t)$ (yellow line), interchangeable solid shaft S1 $M3_{S1}(t)$ (purple line), crank shaft $M4_{J2}(t)$ (green line) and interchangeable hollow shaft S2 $M5_{S2}(t)$ (blue line). The blue dotted blue line is the gravity force on the leaf $M_{F2}(t)$.

6. Discussion

The experimental lab research shows that the variables that have a decisive influence on the magnitude of the dynamic peak forces are mass moment of inertias and accelerations or decelerations in particular. In addition, the external loads acting on the system, such as brake and motor torques or wind load, also have a direct effect. This should come as no surprise, since Newton's laws of physics predict this as well. The other variables, such as stiffnesses, clearances, efficiencies, frictions, etc., have less influence on the magnitude of the dynamic forces or, conversely, have a favorable/damping effect.

The verification measurements showed that the physical system of a movable bridge can be reduced to a series of independent second-order differential equations, each of which corresponds to equations of a linear system with two degrees of freedom. In some load situations, a dynamic model with only one degree of freedom is also sufficient. Moreover, a recursive rule is considered applicable for the calculation of the positions in the dynamic model: new position = old position + displacement. This also applies to the speed of the degrees of freedom: new speed = old speed + acceleration/time step. This

means that at each subsequent time step the change of position and velocity is calculated and must be added to the position and velocity of the previous step, respectively. With this calculation method, various calculation models can be constructed with which the dynamic forces in machineries can be calculated during various load situations. The superposition principle also applies here. This means that the dynamic response to the sum of two signals (load cases) is equal to the sum of the responses to each of those signals separately. In addition, it appears that damping in movable bridge machineries can be taken into account as viscous damping with a damping constant that is speed-dependent.

Furthermore, the dynamic model of an torque controlled prime mover is a semi-definite system, while a speed regulated drive is a definite system. With a semi-definite system, a force is applied to the first inertia, causing it to accelerate/decelerate, depending on the direction of the movement and the load situation. Unlike in the past, nowadays, all prime movers are speed controlled by a frequency converter, which regulates the velocity of the motor according to a given VT diagram. As a result, the external excitation on the first degree of freedom is not a force, but a displacement or velocity, which can be modeled as base-excitation system. Therefore, there is an essential difference in the way these two different drive types should be modelled, which must be taken into account.

In addition, the measurements have shown that different braking systems must be modelled differently. A built-in brake with friction clutches causes a high short-term peak load in the motor shaft, which does not occur with a thruster brake. Due to the short duration, this peak force in the motor shaft will not affect the rest of the powertrain. It is therefore important that the correct braking system of the movable bridge is taken into account, when constructing a calculation model. It can also be concluded that a 'definite' system with an adjusted VT diagram is suitable for calculating the dynamic forces in the event of an emergency stop, when the braking torque is applied at full speed. The deceleration path must be adjusted on the basis of the braking time and a deceleration constant of the braking system. To calculate the deceleration constant with a certain braking torque, only the mass inertia of the first degree of freedom should be taken into account.

Finally, discontinuity in the stiffness matrix of the equations of motion, for instance, due to backlash, recoil after braking or passing through the suspension travel of a spring buffer, can be specified in the calculation models with an if-statement. These type of discontinuities in the stiffness matrix are therefore inherent to the parameters of the dynamic system and should not be regarded as separate load situations as mentioned in the current code NEN 6786.

7. Conclusions

The experimental research at TU Delft has provided us with new insights, when it comes to the occurring dynamic forces in movable bridge machineries. As a result of this, the calculation methodology has been improved, with which the dynamic forces in the powertrain can be predicted more realistically, compared to the current calculation rules in accordance with the Dutch bridge standard NEN 6786.

This calculation method can be used to construct various dynamic models, for each type of movable bridges, operating system configurations, different possibilities in component composition of the powertrain and braking systems.

In addition, the input variables of the calculation model, such as initial conditions and external excitations, can be taken into account, depending on possible load combinations. The new calculation models have also been verified by means of accurate laboratory measurements. The correctness and accuracy of the holistic calculation method is verified experimentally.

In the follow-up study, the contribution of the wind load to the dynamic response should be investigated. This can be modeled with a pulse function (large gust of wind) during accelerating/decelerating from intermediate position.

Wind force can also be modeled as a harmonic excitation, when holding the leaf in any position, to investigate the possibility of resonance [11, 12]. The influence of sudden changes in wind direction is considered inconclusive [13].

We would like to inform the readers that a forthcoming thesis, currently under development, will contain detailed information, including the omitted specifics. This ongoing work will provide a more in-depth exploration of the research and interested readers are encouraged to refer to the thesis once it is completed for a more comprehensive understanding.

Acknowledgments

This experimental research is part of a PhD financed by the Dutch Ministry of Infrastructure and the Environment (Rijkswaterstaat), the Province of South-Holland and Antea Group Netherland. Beside these parties, the test rig was also partly supported by Province of Groningen, Province of Utrecht, Municipalities of Amsterdam and Rotterdam, Prorail, Hollandia Services and Infra, DEMO, SEW-Eurodrive, Flender, SKF, FdGd, Boone BV and Kobout

The authors gratefully acknowledge the crucial contribution of George Bitter from Antea Group and Kees van Beek from DEMO to the development of the measurement system. Additionally, the authors thank Robert de Vries and John Hermsen from TU Delft for their support and the opportunity to perform this measurement campaign.

References

[1] NEN 6786:2001, Rules for the design of movable bridges, *The Netherlands Standardisation Institute*, 2001.
[2] NEN 6786-1:2017+C1:2021, Rules for the design of movable bridges, *The Netherlands Standardisation Institute*, 2017.
[3] Stroosma, D., Dynamics of movable bridges, part i: drive machinery, *RWS directie bruggen*, 1980.
[4] Sektani, K., Tsouvalas, A., Metrikine, A., A mathematical model to quantify dynamic forces in the powertrain of torque regulated movable bridge machineries, *Volume 67, Issue 1 Heron Journal*, 2022.
[5] Koglin, T., Movable Bridge Engineering, *John Wiley & Sons Inc.*, 2003.
[6] Foerster, C. B. G. Movable Bridge Design, *ICE Publishing*, 2003.
[7] Aree, P., Analytical approach to determine speed-torque curve of induction motor form manufacturer data, *Procedia Computer Science*, 86:293-296, 2016.
[8] Delhaes, G., Measurements bridge machinery Post Bridge, *Technical Report, TNO*, 2015.
[9] van Schouten, F., van Vliet, A., and Kaufmann, H., Spread measured of braking torques regarding set values of thrustor disc brakes of movable bridge machineries, *Technical Report, Bouwdienst Rijkswaterstaat, Tilburg*, 1990.
[10] Waarts, P. and van Staalduinen, P., Measurements of damping on six movable bridges, *Technical Report B-90-342, TNO, Rijkswaterstaat*, 1990.
[11] Reij, A. W. F., Wind loads on movable bridges, *IABSE Reports*, 64:539-544, 1991.
[12] Boggs, D. and Dragovich, J., The nature of wind loads and dynamic response, *ACI Special Publications*, 240 (2), 2006.
[13] Vrouwenvelder A., Waarts, P. and van Staalduinen, P., Wind loads on movable bridges, *Technical Report B-90-342, TNO, Rijswijk*, 1990.